

Optical emission spectroscopy of carbon laser plasma ion source

Oguzhan Balki^a, Md. Mahmudur Rahman^a, Hani E. Elsayed-Ali^{a,b,*}^a Department of Electrical and Computer Engineering, Old Dominion University, Norfolk, VA 23529, USA^b Applied Research Center, 12050 Jefferson Avenue, Newport News, VA 23606, USA

ARTICLE INFO

Keywords:

Laser plasma

Ions source

Optical emission spectroscopy

ABSTRACT

Carbon laser plasma generated by an Nd:YAG laser (wavelength 1064 nm, pulse width 7 ns, fluence 4–52 J cm⁻²) is studied by optical emission spectroscopy and ion time-of-flight. Up to C⁴⁺ ions are detected with the ion flux strongly dependent on the laser fluence. The increase in ion charge with the laser fluence is accompanied by observation of multicharged ion lines in the optical spectra. The time-integrated electron temperature T_e is calculated from the Boltzmann plot using the C II lines at 392.0, 426.7, and 588.9 nm. T_e is found to increase from ~0.83 eV for a laser fluence of 22 J cm⁻² to ~0.90 eV for 40 J cm⁻². The electron density n_e is obtained from the Stark broadened profiles of the C II line at 392 nm and is found to increase from $\sim 2.1 \times 10^{17}$ cm⁻³ for 4 J cm⁻² to $\sim 3.5 \times 10^{17}$ cm⁻³ for 40 J cm⁻². Applying an external electric field parallel to the expanding plume shows no effect on the line emission intensities. Deconvolution of ion time-of-flight signal with a shifted Maxwell–Boltzmann distribution for each charge state results in an ion temperature $T_i \sim 4.7$ and ~ 6.0 eV for 20 and 36 J cm⁻², respectively.

© 2017 Elsevier B.V. All rights reserved.

1. Introduction

Laser multicharged ion (MCI) sources are attracting significant interest as they offer a pulsed, high flux source of ions from practically any solid [1]. Carbon ions are used in wide applications that include cancer therapy [2], deposition of diamond-like and carbide thin film [3,4], and ion implantation [5–8]. Carbon ion doping was shown to modify TiO₂ thin films, lowering the band-gap energy from 3.3 eV to 1.8 eV [4], thus, making it photocatalytically active to visible light. Carbon ion implantation on thin Ni film grown on a SiO₂/Si substrate was used for the synthesis of graphene layers on top and under the Ni film [6]. Carbon ion implantation on high temperature growth of heteroepitaxial GeSn/Si and SiSn/Si structures was shown to suppress Sn segregation and precipitation, improve the thermal stability of SiSn supersaturated layers, and prevent dislocation in the formation of loops [7]. In these applications of carbon ions only the singly-charged C¹⁺ ions were used. In some applications, the use of MCIs is attractive since their high potential energy is localized to the surface and they can be accelerated with reduced electrostatic field and bent and focused with reduced magnetic field.

Many techniques are used to probe plasma characteristics such as density n_e , electron temperature T_e , ion temperature T_i , and sheath potential. For pulsed plasma, e.g., laser plasma, diagnostic techniques include optical emission spectroscopy (OES) [9], Thomson scattering [9],

laser interferometry [10], and probing of ion emission from the laser plasma [11]. Laser-target interaction generates transient species such as excited atoms, molecules or ions, which emits radiation that includes the ultraviolet to near-infrared parts of the spectra. Line emission from laser plasma have been extensively used to diagnose n_e and T_e [12]. OES is widely used to probe n_e using Stark broadening of spectral lines, for n_e values ranging between 10¹⁴ and 10¹⁸ cm⁻³, and to probe T_e using the ratio of integrated line intensities based on the Boltzmann's method for plasma in local thermal equilibrium (LTE) [13,14].

Several studies were conducted on carbon laser plasma. OES of carbon laser plasma in air generated by an Nd:YAG laser (pulse width $\tau = 5$ ns, frequency $F = 10$ Hz, wavelength $\lambda = 1064$ nm, maximum pulse energy $E = 130$ mJ/pulse, and for $\lambda = 532$ nm, maximum $E = 72$ mJ/pulse) [12]. The electron density n_e was calculated from the Stark broadening profile of the C I line at 247.85 nm. The electron temperature T_e was calculated from the neutral C I lines at 247.85, 394.22, 396.14, 588.95, and 591.25 nm. At a distance of 0.05 mm from the target surface, n_e was reported as 4.6×10^{17} cm⁻³ for 130 mJ at $\lambda = 1064$ nm, and 5.98×10^{17} cm⁻³ for 72 mJ at $\lambda = 532$ nm. The corresponding T_e values were 0.85 and 0.81 eV for the $\lambda = 1064$ and 532 nm laser radiance, respectively [15]. For ablation of graphite by an Nd:YAG laser ($\lambda = 1064$ nm, $F = 10$ Hz, intensity $I = 59$ GW cm⁻²), n_e

* Corresponding author at: Department of Electrical and Computer Engineering, Old Dominion University, Norfolk, VA 23529, USA.
E-mail address: helsayed@odu.edu (H.E. Elsayed-Ali).

and T_e were reported as $2.1 \times 10^{17} \text{ cm}^{-3}$ and 2.43 eV, respectively, at a distance 1 mm from the surface of the target decaying to $1 \times 10^{17} \text{ cm}^{-3}$ and 1.6 eV at 11 mm from the target surface for a laser radiance of 59 GW cm^{-2} [12]. Dual-laser ablation of carbon plasma ($\tau = 7 \text{ ns}$, 10 Hz, $\lambda_1 = 1064 \text{ nm}$, $\lambda_2 = 532 \text{ nm}$ at fluence of 25 and 17 J cm^{-2} , respectively) showed up 5 fold intensification of C II emission lines for a delay of 500–1000 ns between the two laser pulses [16]. Changing the delay between the two laser pulses was shown to affect the ion kinetic energy. Ion time-of-flight (TOF) measurement and UV spectroscopy were conducted for the Al, Ti, Mo, and Au plasmas generated by irradiation with a Nd:YAG laser ($\tau = 3 \text{ ns}$, single-shot or up to 10 Hz, $\lambda = 1064 \text{ nm}$, at a fluence up to 18 J cm^{-2}) [17]. They probed the plasma plume by optical spectroscopy and deconvolution from TOF. For ablating with 18 J cm^{-2} , the reported ion temperatures for Al, Ti, Mo, Au, were 40, 41, 42, 44 eV, respectively. These values were obtained from deconvolution of the ion TOF signal based on a shifted Coulomb–Boltzmann distribution. The electron temperatures reported with optical spectroscopy were in the order of 1.0 eV. The difference in T_i and T_e was attributed to the different zones of the laser plasma where the ions and optical radiation were generated at [17].

We report on a combined OES and ion TOF study of carbon plasma generated by laser ablation using an Nd:YAG laser operating at $\lambda = 1064 \text{ nm}$ with $\tau = 7 \text{ ns}$. Time-integrated T_e and n_e are measured by OES, while ion TOF is used to obtain T_i . Carbon spectral lines up to C IV (C^{3+}) and carbon ions with charge states up to C^{4+} are observed for ablation by a laser fluence of $\geq 27 \text{ J cm}^{-2}$. The Stark-broadened profile of the singly-ionized C II line at 392.0 nm is used for the measurements of n_e , while the relative line intensities of the C II lines at 392.0, 426.7, and 588.9 nm are used to calculate T_e . Applying an external electric field parallel to the direction of plume propagation increases the carbon MCI extraction, however, no change in the carbon emission lines was observed.

2. Experimental

A schematic of the experimental setup is shown in Fig. 1. The vacuum chamber has a background pressure of $\sim 2 \times 10^{-8} \text{ Torr}$. At such pressure, the loss of MCIs by charge transfer to the background gas over the transport line length is negligible [18]. A Q-switched Nd:YAG laser (Continuum Surelite SL I-10, $\tau = 7 \text{ ns}$, $\lambda = 1064 \text{ nm}$, $F = 4 - 52 \text{ J cm}^{-2}$) is used for plasma generation from a glassy carbon disk target of 5.8 mm thick, 99.99% purity, <50 nm surface roughness. The carbon target is electrically insulated from the chamber to allow applying a positive bias while the chamber is grounded. The laser pulse energy is controlled by a half-wave plate and a polarizing beam splitter. The laser pulse is incident on the target at an angle of 60° from the target normal and focused using a lens with a focal length of 200 mm to an elliptical spot on the surface of the target with an area of 0.1256 mm^2 . The laser spot size was measured by scanning the laser spot with a knife edge parallel and perpendicular to the spot's major axis at target-equivalent plane in a direction 60° from the beam propagation direction. The reported laser fluences are adjusted for the losses in the BK7 glass window and the lens. A grounded nickel mesh 8 cm in diameter with an open area of 70% is placed 10 cm in front and parallel to the surface of the carbon disk. A voltage of 0–9 kV is applied to the carbon target using a high-voltage power supply (CPS Inc., 100-R, 30 kV, 1 mA) while keeping the chamber grounded. Ions with a range of kinetic energy-to-charge E/z ratios are selected by an electrostatic ion energy analyzer (EIA) with a radial cylindrical design at a deflection angle of 90° . The EIA has a range of E/z obtained by the relation $E/z = eU/[2 \ln(R_2/R_1)]$, where E is the kinetic energy of the ion, e is the electron charge, U is the total potential across the plates, R_1 is the inner radius, and R_2 is the outer radius [19,20]. Ion entrance and exit slits can be placed in the EIA to reduce the spread in E/z selected. All results reported are without slits in order to increase ion transmission. The ions are detected by a Faraday cup (FC) made out of Al and placed 154 cm away from

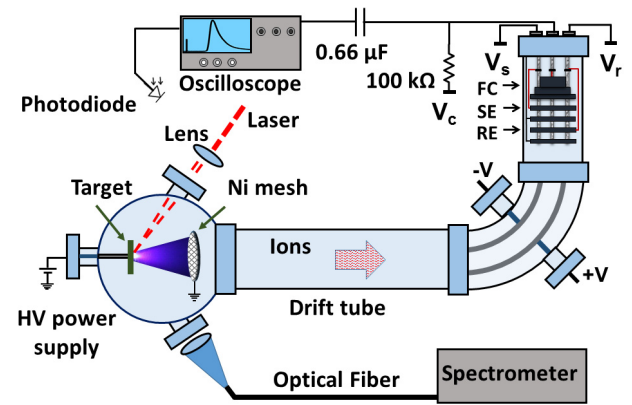


Fig. 1. A schematic of the experimental setup. The laser multicharged ion (MCI) chamber is connected to with a transport line with electrostatic ion analyzer (EIA), three-mesh retarding field analyzer (RFA), and time-of-flight (TOF) analyzer. V_r , V_s , and V_c are the voltage applied to the retarding electrode (RE) of the three-grid energy analyzer, suppressor electrode (SE), and Faraday cup (FC).

the carbon target. The ion transport line is a stainless-steel tube with 10 cm ID. The signal from secondary electron emission is suppressed by a suppressor ring electrode that is 5 cm in diameter placed 1 cm away from the FC entrance. The MCI TOF signal is detected with the FC biased at -80 V . The secondary electron emission signal from the FC due to positive ion collisions is found to be completely suppressed when biasing the suppressor electrode at -120 V . More details on the experimental setup were previously reported [21]. An oscilloscope (Tektronix DPO 3034, 50Ω termination) records the carbon ion signals through a $0.66 \mu\text{F}$ coupling capacitor. For MCI TOF data collection, twenty consecutive laser pulses hitting the same target area are averaged in order to increase the signal-to-noise ratio. An optical spectrometer (Avantes, ULS3648) is used to record the spectral lines emitted from the carbon plasma. The carbon spectral emission is recorded through an optical fiber (Avantes, FC-UV-1000-1-ME) placed $\sim 15 \text{ cm}$ away from the target at an angle of 60° from the target normal. The laser is operated at 10 Hz. The optical spectra are obtained by integrating for 20 s in a dark room. Background noise was recorded before any spectrum was acquired and subtracted from the optical spectra. The effect of applying an external electric field on the optical spectra is probed with another optical spectrometer (Avaspec-3648). This spectrometer covers the spectral range of 185–750 nm. In that case, the laser is operated at 1 Hz, while each spectrum is obtained by integrating the optical signal for 10 s. In this case, the optical feedthrough is replaced with a quartz viewport and a lens with focal length of 200 mm is used to image the plume onto the fiberoptic cable entrance.

3. Results and discussions

3.1. Optical emission spectra

In this section, time-integrated optical emission spectra of the laser plasma are discussed. The effects of the laser fluence on the electron density n_e and electron temperature T_e are reported. We also report on the optical emission spectra when an external electric field is present across the laser plasma.

3.1.1. Lines intensities

The optical emission spectra obtained for different laser fluences are shown in Fig. 2. The carbon laser-plasma consists of ionization emission lines of C II, C III, and C IV transitions. A particular feature for the higher laser fluences is the increase in the intensities of all carbon lines and generation of higher ionization states. The line profile of the C^{1+} ion (C II at 392.0 nm) is used for the electron density n_e calculations. For

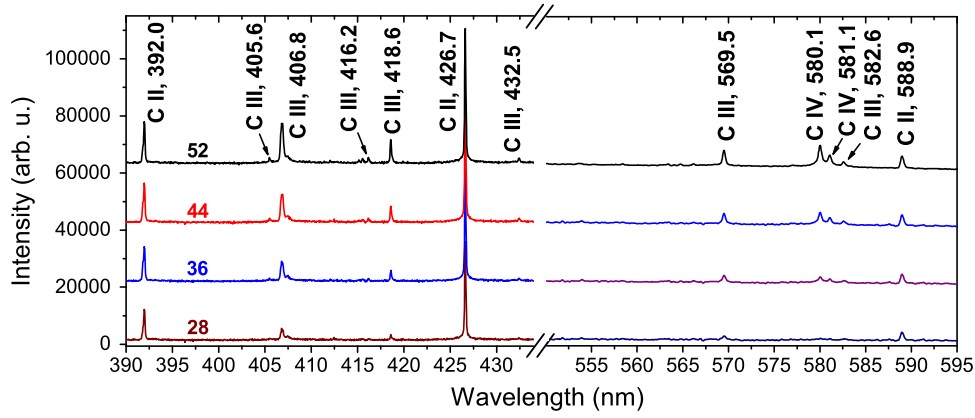


Fig. 2. Carbon laser plasma spectra acquired over the wavelength range 390–595 nm. The laser pulse fluence is indicated on top of each spectrum.

a laser fluence at 28 J cm^{-2} , C II transitions at 392.0, 426.7, and 588.9 nm, and weak C III lines at 406.8, and 569.5 nm are observed. As the fluence is increased, the C III transitions at 405.6, 406.8, 416.2, 418.6, 432.5, 569.5, 582.6 nm, and C IV transitions at 580.1, and 581.1 nm are detected. While all line intensities depend on the laser fluence, the C IV lines are most affected by the laser fluence.

3.1.2. Electron density

For high density plasmas, such as for laser plasma, OES is often used to probe the electron density n_e based on Stark broadening of emission lines [22]. For our calculations, we use the profile of the C II 392.0 nm line to determine the electron density n_e [23]. Harilal et al. studied carbon laser plasma for similar laser conditions ($\lambda = 1064 \text{ nm}$ and $E = 275 \text{ mJ}$) and reported that the effects of pressure and Doppler broadening on the linewidth of the C II line at 392 nm are negligible compared to that of Stark broadening [12]. Stark broadening in plasmas occurs due to collisions of the emitting neutral or ion with charged particles, which results in a shift in the peak wavelength, and a broadening of the line. The full-width at half-maximum (FWHM) of the Stark-broadened lines $\Delta\lambda_{1/2}$ is related to n_e by [14]:

$$\Delta\lambda_{1/2} = 2w \left[\frac{n_e}{10^{16}} \right] \quad (1)$$

where w is the electron impact broadening parameter in Å and n_e is the electron number density in cm^{-3} . The value of w is retrieved from Griem as 0.0245 Å depending on the plasma temperature T_e of 0.86 eV ($10,000 \text{ K}$) for C II line ($\lambda = 392.0 \text{ nm}$, $4s^2S_{1/2} \rightarrow 3p^2P_{3/2}$ transition) assuming local thermodynamic equilibrium (LTE) [14]. For n_e to satisfy LTE, the condition $n_e \geq 1.4 \times 10^{14} T_e^{1/2} (\Delta E_{ji})^3 \text{ cm}^{-3}$ must be valid, where ΔE_{ji} is the energy difference between the upper and the lower levels of the transition [23]. This is a necessary, but insufficient condition for LTE. For the transition of C II at 392.0 nm $\Delta E_{ji} = 3.16 \text{ eV}$, and the lowest limit for n_e is $5.4 \times 10^{15} \text{ cm}^{-3}$ for $T_e = 1.5 \text{ eV}$ [23,24]. In our calculation, correction was made for the instrumental broadening of 0.09 nm , as measured by the FWHM of the Hg 435.8 nm line from a low pressure Ar–Hg lamp. The line width is determined by a numerical fit of a Lorentzian profile to the measured C II line profiles at 392.0 nm. Fig. 3 gives the variation of electron density n_e of the carbon plasma with the laser fluence. With an increase in the laser fluence from 4 to 40 J cm^{-2} , the calculated n_e increases from $\sim 2.1 \times 10^{17}$ to $\sim 3.5 \times 10^{17} \text{ cm}^{-3}$. The saturation in n_e at the higher laser fluences is due to plasma shielding by the reflection or absorption of the laser photons by the expanding carbon plasma [12,25].

3.1.3. Electron temperature

The C II 392.0, 426.7, and 588.9 nm lines are used for electron temperature T_e calculation. Considering the detected carbon species, these lines have the biggest difference between their corresponding

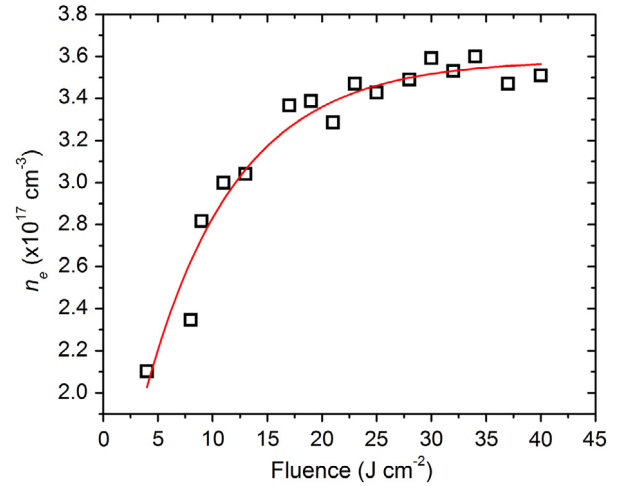


Fig. 3. The variation of n_e with the laser fluence. The line profiles of C II at 392.0 nm is used to determine the electron density n_e .

upper energy levels, and provide the best straight line fit in the Boltzmann plot, which led to better accuracy in T_e determination from the Boltzmann plot [26]. The corresponding upper energy level transitions E_j for these lines are 157, 234.07, 168, 978.34, and 162, 524.57 cm^{-1} , respectively [27]. Since the lowest electron density observed in Fig. 3 is $2.1 \times 10^{17} \text{ cm}^{-3}$, the n_e satisfies the local thermodynamic equilibrium (LTE), and for laser plasma, T_e can be determined from the Boltzmann plot method [14,15]. The fitting parameters of the Lorentzian function to the line profile affects the deduced electron density n_e . The following relation is used for T_e calculations [15]:

$$\ln \left[\frac{\lambda_{ji} I_{ji}}{g_j A_{ji}} \right] = \ln \left[\frac{N(T)}{U(T)} \right] - \frac{E_j}{k T_e}, \quad (2)$$

where, λ_{ji} is the transition wavelength, I_{ji} is the temporally and spatially-integrated line intensity of the transition involving the upper level j and the lower level i , g_j is the statistical weight of the level j , A_{ji} is the transition probability, $N(T)$ is the total number density, $U(T)$ is the partition function, E_j is the energy of the upper level, k is the Boltzmann constant, and T_e is the excitation temperature. A plot of $\ln(\lambda_{ji} I_{ji} / g_j A_{ji})$ versus the energy E_j for the observed spectral lines follows a straight line and its slope $-1/kT_e$ gives the T_e . Spectroscopic parameters (λ_{ji} , A_{ji} , g_j , E_j), listed in Table 1 are obtained from the NIST database [27].

The calculated T_e are reported in Fig. 4. The value of T_e for the plasma produced at 24 J cm^{-2} fluence is presented in the inset of Fig. 4 as $\sim 0.85 \text{ eV}$ calculated using C II (392.06, 426.72, and 588.97 nm) lines. When the laser pulse fluence is increased from 22 to 40 J cm^{-2} , the T_e

Table 1
Spectroscopic parameters of C II transition lines [27].

Wavelength λ (nm)	Transitions	Statistical weight g_j	Transition probability A_{ji} (s^{-1})	Upper level energy E_j (cm^{-1})
392.06	$4s^2S_{1/2} \rightarrow 3p^2P_{3/2}$	2	1.27×10^8	157,234.07
426.72	$4f^2F_{7/2} \rightarrow 3d^2D_{5/2}$	8	2.38×10^8	168,978.34
588.97	$4p^2P_{3/2} \rightarrow 3d^2D_{5/2}$	4	3.15×10^7	162,524.57

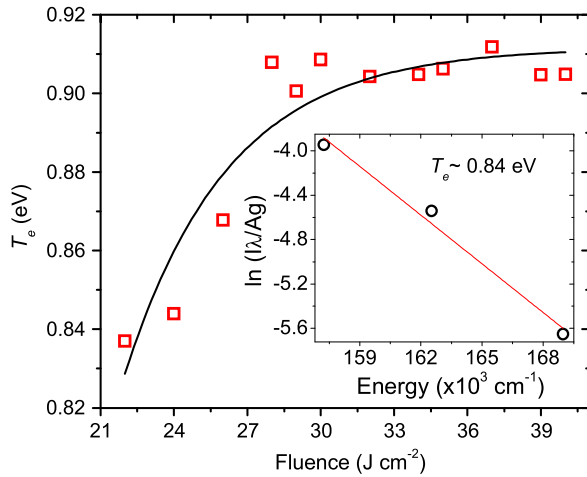


Fig. 4. Electron temperature T_e variation with laser pulse fluence range of 22–40 $J\,cm^{-2}$. Inset is electron temperature T_e for laser fluence of 24 $J\,cm^{-2}$ calculated using C II lines at 392.0, 426.7, and 588.9 nm with the Boltzmann plot method. The solid line shows a linear fit of the experimental data from where the slope is determined.

increases from ~ 0.83 eV to ~ 0.90 eV, where a saturation is observed for ≥ 32 $J\,cm^{-2}$ laser fluence. Hanif et al. reported T_e values with the Boltzmann plot method for carbon plasma generated by an Nd:YAG laser ($\lambda = 1064$ nm, $E = 400$ mJ, $\tau = 5$ ns, and $\lambda = 532$, $E = 200$ mJ,) as ~ 0.85 eV and ~ 0.81 using the C I neutral lines [15]. The laser-generated plasma is affected by the laser parameters (wavelength, pulse duration, and intensity) and the physical properties of the material [28]. Both n_e and T_e measurements are reported for time-integrated signals measured at an angle of 60° from the target normal. The spatial variations of the rapidly varying electron temperature T_e was not considered due to the collection of data from a fixed angle.

3.1.4. Effect of external electric field on optical spectra

We studied the effect of applying an external electric field to the expanding plasma plume. A voltage of 6 kV is applied to the carbon target, which introduces an electric field between the grounded mesh and the target. The optical spectra was measured with the target at 0, 2, 4, and 6 kV. The applied electric field had no observable effect on the intensity of the C II, III, and IV spectral lines, as shown in Fig. 5, in which the optical spectra are given with the target grounded and when 6 kV is applied to the target. Variations in the line intensities are believed to be within the experimental errors. There is also no noticeable change in the number of carbon lines or line profiles with the applied voltage up to 6 kV. The lines at 495.5 and 610.3 nm may be due to impurities from oxygen. Additional measurements of current and voltage on the positively-biased target are conducted using a current pick-up coil (Pearson 6595) and a fast high-voltage probe (Tektronix, P6015A). The IV measurements show that the plasma is shorted through the grounded mesh with current flowing through the mesh. For the present experimental conditions, the optical emission line intensities and profiles were not affected by the electric field set between the target and the grounded mesh. A stainless steel target, mounted in the middle of a two parallel plate charged capacitor, was irradiated by an Nd:YAG laser ($\lambda = 1064$ nm, $\tau = 7$ ns, $E = 350$ mJ) in air. No change in the shape and intensity of the emission spectra was observed in applied electric fields up to $10\,kV\,cm^{-1}$ [29]. An enhancement in the electron

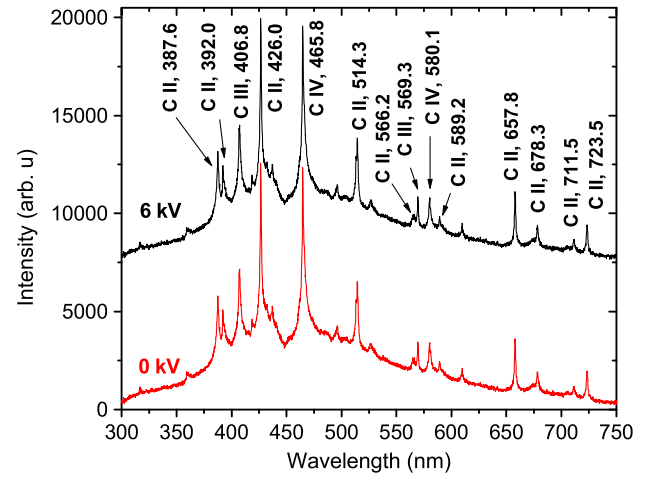


Fig. 5. Optical emission spectra of carbon laser plasma expanding in an external electric field. The carbon target is grounded for the lower spectrum and biased to 6 kV for the upper spectrum.

temperature with the application of a 140 MHz radio-frequency electric field to laser plasma with the electron temperature increasing from 0.3 to 1.0 eV when 1.0 W radiofrequency power was applied [30]. For laser plasma generated by ablation of $YBa_2Cu_3O_7$ by an ArF excimer laser ($\lambda = 193$ nm) in an oxygen environment, applying an electric field in the plume propagation direction enhanced emission lines [31].

3.2. Ion time-of-flight

The carbon ions emitted from the plasma plume when the target is grounded or positively biased were observed. The effects of the laser pulse energy on the ion charge, charge state, and ion temperature T_i is studied for a grounded target. When the target is positively biased, we used the electrostatic ion analyzer EIA to select ions with a specific energy-to-charge ratio E/z . The effects of the laser pulse energy and applying voltage to the target on the ions generation are studied.

3.2.1. Ion signal for grounded carbon target

The kinetic energy distribution of ions emitted from the laser plasma is often used to obtain the ion plasma temperature in the core of the plume, where these ions are mostly generated [17]. The electrons are accelerated by inverse bremsstrahlung within the laser pulse duration and gain higher speeds with forward and lateral directions establishing an electric field at the plasma–vacuum interface due to charge separation [32]. In the early stages of the plasma plume formation, large Coulomb forces are formed between these fast electrons and ion layers due to the slower mobility of ions compared to the electrons. The electric field due to the Coulomb forces accelerates ions with a higher degree of ionization to higher kinetic energies [33]. Some ions recombine with electrons as they travel forward and form either neutrals or low charge-state ions [34].

The carbon ions are detected by the Faraday cup FC. All other conditions except the pulse fluence are kept constant for the measurements conducted. The ions with higher kinetic energies are located in the front of the plasma plume due to their higher drift velocities. Ion TOF signals are shown in Fig. 6. In this configuration, the EIA is replaced with a straight tube, while maintaining the ion drift length the same. The ion

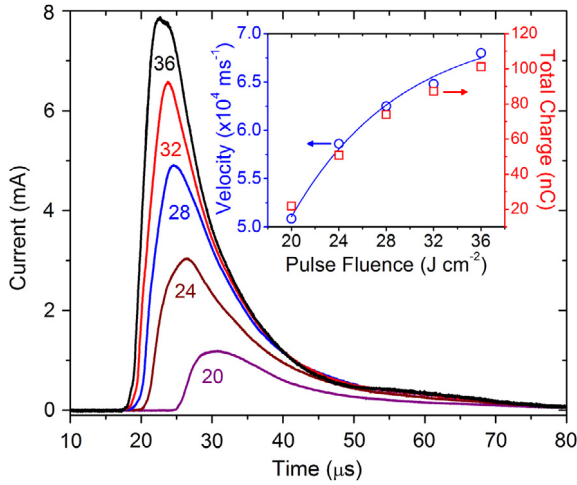


Fig. 6. Time-of-flight ion detection from carbon laser plasma for different laser pulse fluence (J cm^{-2}). Inset shows the total ion charge and most probable ion velocities with the increase of laser pulse fluence.

signals have a well-defined single peak. There is an apparent reduction in the arrival time of the fast ion peak with the increase in the laser pulse fluence. This behavior of TOF signal with increasing laser pulse fluence indicates an increase in ion signal and a shortened arrival time due to the increased ion energy. The total charge detected by the FC is increased from ~ 22 to ~ 101 nC when the laser fluence is increased from 20 to 36 J cm^{-2} . For a laser pulse fluence higher than 28 J cm^{-2} , the increase in ion velocity slows down. For 32 J cm^{-2} fluence, the most probable carbon ion velocity is $\sim 6.5 \times 10^4 \text{ m s}^{-1}$, corresponding to a kinetic energy of $\sim 262 \text{ eV}$, shown in the inset of Fig. 6.

3.2.2. Ion temperature for grounded carbon target

For our laser ablation conditions, the laser plasma can be described as having an achieved LTE [13]. Under these conditions and considering the double-layer potential developed between the expanding plume and vacuum interface, the ion velocity distribution emitted from the plasma plume follows a shifted Maxwell-Boltzmann (SMB) distribution [33,35]. TOF ion signals are fitted to a SMB distribution function $I(t) = At^{-5} \exp[-m((L/t) - u_f)^2 / 2kT_i]$, where A is a normalizing constant, m is the atomic mass of carbon, L is the distance from the target to the Faraday cup, u_f is the flow velocity, k is the Boltzmann constant, and T_i is the ion temperature associated with translational motion along the plume axis [33]. Achieving ions with SMB distribution assumes the thermalization of the plume particles and that the flow velocity u_f is fixed after a short distance from the target [28,33]. The background pressure in the laser ablation chamber and in the ion transport line must be sufficiently low to allow ion drift with negligible recombination. The total scattering cross section for ions with different charge states was reported previously [36]. From these cross sections, the mean-free-path of the carbon ions for background pressure of 3×10^{-8} Torr is $\geq 1.8 \times 10^3 \text{ m}$. Ion recombination in the drift tube is negligible since the drift distance of the carbon ions from the target to the Faraday cup is 1.54 m . The ion charges are frozen and the SMB distribution is applicable for ions drifting in vacuum for these conditions [37,38]. We previously reported on the deconvolution of TOF signal for carbon and aluminum ions [20,39,40]. For laser pulse fluence of 28 J cm^{-2} , carbon ions up to C^{2+} are used for the SMB fitting, while for a laser pulse fluence of 120 J cm^{-2} ions up to C^{4+} are used for the fit [20]. Aluminum ablation with a fs laser ($\lambda = 800 \text{ nm}$, $\tau = 100 \text{ fs}$, $I = 10^{13} - 10^{14} \text{ W cm}^{-2}$) showed that equivalent ion temperature was 25 eV for a grounded Al target at 7.6 J cm^{-2} pulse fluence [40]. In one study [41], ions generated from tin laser plasma using a Q-switched Nd:YAG laser ($\lambda = 1064 \text{ nm}$, $\tau = 5 \text{ ns}$, $I \sim 10^{11} \text{ W cm}^{-2}$) were fitted to SMB

distribution and the reported T_i was 34.4 eV for 77 mJ pulse energy. The ion pulse that contains contributions of ions with different charges is deconvolved into separate signals each corresponding to a charge state with its own SMB distribution. The sum of these signals is fitted to the TOF signal from all ions [41]. Another study reported on the expansion dynamics of Al plasma generated by ns Nd:YAG ($\lambda = 1064 \text{ nm}$, $\tau = 7 \text{ ns}$) and a Ti:sapphire laser ($\lambda = 796 \text{ nm}$, $\tau = 100 \text{ fs}$) pulses using SMB fitting to ion TOF signal [28]. A reasonable fitting was achieved, which indicates mostly thermal contributions to the velocity. Flow velocity $u_f = 14.4 \times 10^3 \text{ m s}^{-1}$ and an ion temperature $T_i = 21.96 \text{ eV}$ was retrieved from the fit. For ablation with a 7 ns laser pulse, two ion velocity components (slow and fast) were present in the TOF signal. While the slow component showed a good fit with $u_f = 5 \times 10^3 \text{ m s}^{-1}$ and $T_i = 1.74 \text{ eV}$, the fast component was fitted better with a Gaussian distribution, an indication that the fast peak had a non-thermal nature [28,42]. Bulgakova et al. reported $T_i = 6.46 \text{ eV}$ for a graphite target ablated with an Nd:YAG laser ($\lambda = 1064 \text{ nm}$, $\tau = 13 \text{ ns}$, $F = 16 \text{ J cm}^{-2}$) [33]. They suggested that the TOF is poorly described for a low laser fluence due to the non-Maxwellian tail in the signal [33].

Fig. 7 shows the ion TOF signal and corresponding SMB deconvolution fits. The sum of individual fitting curves from the carbon ions compose the total ion current. The tails in Fig. 7(a) and (b) at the longer time indicate the presence of slow C^{1+} (C_s^{1+}) ion components that contribute to the TOF signal. When the slow C^{1+} ions are considered, a better fit to the data was achieved. For a laser pulse fluence of 36 J cm^{-2} as in Fig. 7(a), we determined u_f from the SMB fit as $3.6 \times 10^4 \text{ m s}^{-1}$ for C^{1+} and $2.0 \times 10^4 \text{ m s}^{-1}$ for C_s^{1+} , whereas for a lower pulse fluence of 20 J cm^{-2} as in Fig. 7(b), the value of u_f decreased to $3.4 \times 10^4 \text{ m s}^{-1}$ for C^{1+} and $1.6 \times 10^4 \text{ m s}^{-1}$ for C_s^{1+} , respectively. The equivalent T_i of the ejected ions obtained by the ion TOF deconvolution in Fig. 7(a) and (b) are 6.0 and 4.7 eV , respectively, when no accelerating voltage is applied.

3.2.3. Ion emission for plume expanding in external electric field

We next report on the carbon ion TOF signal when different voltages are applied to a carbon target. Due to the double-layer potential and the externally applied electric field, ions with different charges spread in time with the higher charge states arriving at the FC earlier. The TOF for the carbon ions is $t_a + t_d = d\sqrt{2m/zeV} + s\sqrt{m/2zeV}$, where t_a is the acceleration time for an ion from target to the extraction mesh, t_d is the time that ions drift at a constant velocity from the extraction mesh to the FC, d is the distance between target and the extraction mesh, S is the total distance from the extraction mesh to the FC, both in meters, m is the atomic mass of C in kg, z is the charge state, e is the electron charge, and V is the biasing voltage applied on the carbon target. The initial ion velocity from the plasma plume, mainly due to the double-layer potential, is neglected in this equation as it is much smaller than the velocity component due to the applied potential considered here. This equation also does not account for the effect of plasma shielding limiting the ion acceleration by the external electric field and the adiabatic ion acceleration in the expanding plasma plume. Introducing an external electric field increases the kinetic energy of ions, thus temporal separation of ions, according to their charge state, occurs. Fig. 8(a) shows carbon signal detected by the FC after the ions pass the EIA. C^{1+} is easily generated because the amount of energy to remove the loosely bound electron is already contained within the laser carbon plasma. Considering the similar C^{1+} intensity profiles recorded, it is also possible that most of the C^{1+} ions are converted to C^{2+} ions since the ionization energy levels are comparable by a factor of 2. We observed C^{1+} , C^{2+} , and C^{3+} for target voltages below 5 kV . C^{4+} is observed along with lower charge states when the target voltages are 5 kV or more. The electric field between the grounded mesh and the target does not penetrate the plasma plume and affects only the lower density outer part of the plume. Thus the ions experience the applied electric field at a location between the target and the mesh, and therefore, are accelerated less than the potential applied to the target. Energy-to-charge selection E/z is adjusted according to the applied voltage on

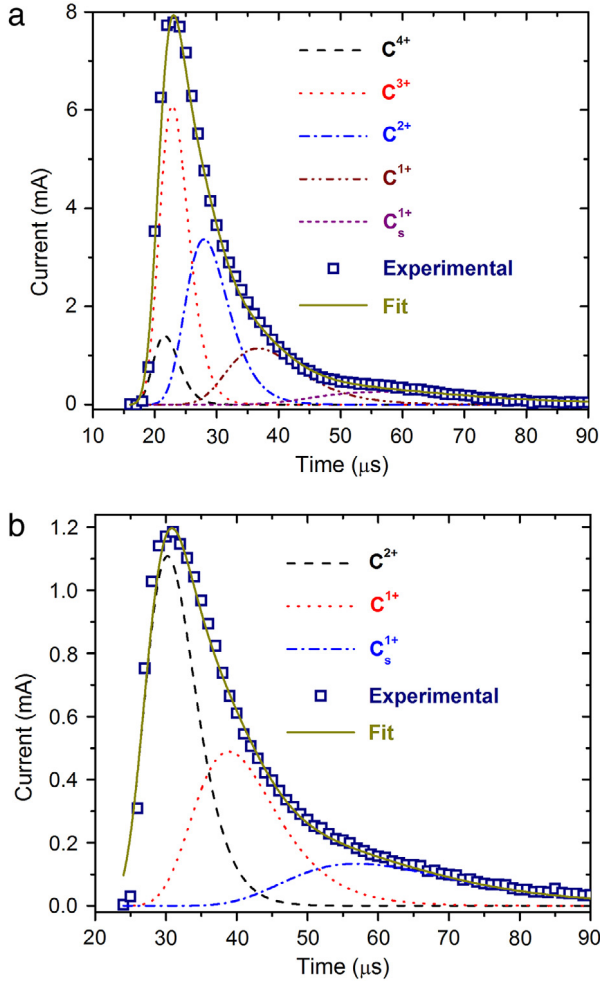


Fig. 7. Deconvolution of the TOF signal from C ions into different ion charges each following the SMB distribution. C_s^{1+} refers to the slow ion component of the singly-ionized carbon ion. The laser pulse fluence is 36 J cm^{-2} (a) and 20 J cm^{-2} (b).

target to maximize the detected ion current. We previously reported that the energy resolution $\Delta E/E$ was determined to be 7–10% because no slit was used on both ends of the EIA [20]. Nassisi et al., showed that introducing two gaps for ion acceleration in a laser ion source reduces the breakdown through the grounded chamber walls and increases the efficiency of ion delivery [43]. For 60 kV acceleration voltage and ablating the targets with a laser operating at $\lambda = 248 \text{ nm}$ with intensity of the order of 10^8 W cm^{-2} , peak ion currents of 5.7, 7.3, and 15.0 mA were obtained by laser ablation of Cu, Y and Ag targets, respectively [43].

The carbon ions detected by the Faraday cup are strongly dependent on the laser pulse fluence which increases the electron density n_e and temperature T_e allowing for the generation of higher state carbon ions. The dependence of ion generation on the laser pulse fluence is studied for a target voltage of 9 kV and the EIA voltage selected for $E/z = 5.3 \text{ keV}$, which provides maximum signal as detected by the FC. The ion signal obtained at laser pulse fluence from 24 to 40 J cm^{-2} are shown in Fig. 8(b). We observe that the threshold pulse fluence for the carbon ion detection is 5 J cm^{-2} per pulse. C^{1+} and C^{2+} ions are always observed for pulse fluence above 5 J cm^{-2} . The average charge state, peak ion energies, and corresponding intensities are increased accordingly with the laser pulse fluence. For laser pulse fluence above 24 J cm^{-2} , C^{4+} ions are also generated. We did not observe C^{5+} or C^{6+} at these laser pulse fluence. The reduced TOF with the laser pulse fluence observed in Fig. 8(b) is due to the increase in kinetic energy of the ions drifting out of the expanding plasma. The inset of Fig. 8(b) shows the total ion

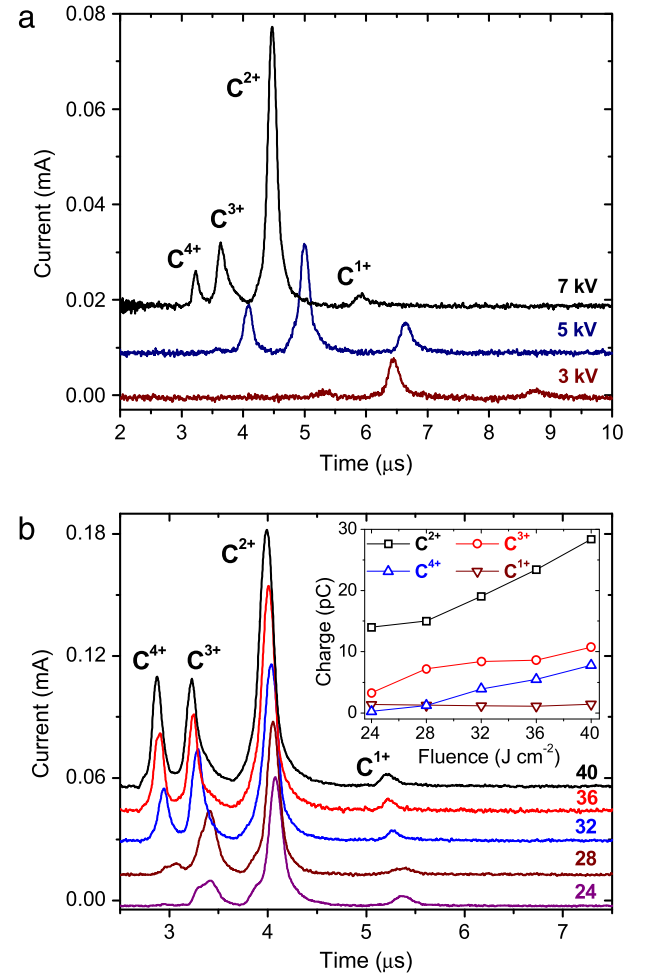


Fig. 8. Carbon ions charge state generation at different biasing voltage applied on carbon target at 32 J cm^{-2} laser pulse fluence (a). Energy-to-charge selection E/z is adjusted accordingly to maximize the detected ion current: $E/z = 1.8, 3.2$, and 4.3 keV for 3, 5, and 7 kV, respectively. Carbon ion generation with increasing laser fluence at $E/z = 5.3 \pm 0.3 \text{ keV}$, and 9 kV applied to target (b). Results indicate up to C^{4+} can be extracted with 40 J cm^{-2} fluence. Inset is charge detected for each carbon ion.

charge dependence on the laser pulse fluence for each carbon ion charge generated. The total charge detected by the FC increases with the laser pulse fluence having the most contribution from C^{2+} ions. The total charge recorded for 40 J cm^{-2} pulse fluence are 1.4 pC for C^{1+} , 28.4 pC for C^{2+} , 10.7 pC for C^{3+} , and 7.8 pC for C^{4+} .

4. Conclusion

Carbon ions and spectral emission lines are measured for ablation using a Q-switched Nd:YAG laser. We observed carbon MCIs up to C^{4+} at 3 kV target voltage and carbon spectral lines up to C IV for laser pulse fluence above 28 J cm^{-2} . The kinetic energy of the carbon ions is 5.3 keV per charge for 9 kV target voltage. The electron temperature T_e of $\sim 0.90 \text{ eV}$ for C II lines is calculated using the Boltzmann plot method for ablation with a laser fluence of $\sim 40 \text{ J cm}^{-2}$. Deconvolution of the carbon ion signal using SMB distribution for TOF signals gives an ion plasma temperature $T_i \sim 6.0 \text{ eV}$ for 36 J cm^{-2} . The OES and ion TOF reveal different plasma temperatures due to the probing of different plasma regions. The electron density n_e was $\sim 2.1 \times 10^{17} \text{ cm}^{-3}$ to $\sim 3.5 \times 10^{17} \text{ cm}^{-3}$ for laser pulse fluence of 4 to 40 J cm^{-2} and saturates for a fluence $> 25 \text{ J cm}^{-2}$. We also investigated the influence of applying an external electric field of up to 600 V/cm on the carbon emission lines with no noticeable change observed.

Acknowledgment

This research was supported by National Science Foundation under Grant No. MRI-1228228.

References

- [1] K. Bernhardt, G. Fuchs, M.A. Goldman, H.C. Herbert, D. Obermann, W. Walcher, K. Wiesemann, Studies of electron heating and multiply charged ion production in an electron cyclotron resonance plasma, *Plasma Phys.* 18 (1976) 77–94.
- [2] T. Kamada, H. Tsujii, E.A. Blakely, J. Debus, W. De Neve, M. Durante, O. Jäkel, R. Mayer, R. Orecchia, R. Pötter, S. Vatsitsky, W.T. Chu, Carbon ion radiotherapy in Japan: an assessment of 20 years of clinical experience, *Lancet Oncol.* 16 (2015) e93–e100.
- [3] W. Ensinger, Correlations between process parameters and film properties of diamond-like carbon films formed by hydrocarbon plasma immersion ion implantation, *Surf. Coat. Technol.* 203 (2009) 2721–2726.
- [4] A.V. Semenov, V.M. Puzikov, A laboratory setup for obtaining silicon carbide films by the direct ion deposition method, *Instrum. Exp. Tech.* 53 (2010) 761–765.
- [5] G. Impellizzeri, V. Scuderi, L. Romano, E. Napolitani, R. Sanz, R. Carles, V. Privitera, C ion-implanted TiO₂ thin film for photocatalytic applications, *J. Appl. Phys.* 117 (2015) 105308–6.
- [6] J. Kim, G. Lee, J. Kim, Wafer-scale synthesis of multi-layer graphene by high-temperature carbon ion implantation, *Appl. Phys. Lett.* 107 (2015) 033104–4.
- [7] P.I. Gaiduk, J. Lundsgaard Hansen, A. Nylandsted Larsen, F.L. Bregolin, W. Skorupa, Suppression of tin precipitation in SiSn alloy layers by implanted carbon, *Appl. Phys. Lett.* 104 (2014) 231903–5.
- [8] M. Uhl, M. Mattke, T. Welzel, F. Roeder, J. Oelmann, G. Hahl, A. Jensen, M. Ellerbrock, O. Jäkel, T. Haberer, K. Herfarth, J. Debus, Highly effective treatment of skull base chordoma with carbon ion irradiation using a raster scan technique in 155 patients: First long-term results, *Cancer* 120 (2014) 3410–3417.
- [9] E.A.D. Carbone, S. Hübner, M. Jimenez-Diaz, J.M. Palomares, E. Iordanova, W.A.A.D. Graef, A. Gamero, J.J.A.M.v.d. Mullen, Experimental investigation of the electron energy distribution function (EEDF) by Thomson scattering and optical emission spectroscopy, *J. Phys. D: Appl. Phys.* 45 (2012) 475202.
- [10] H.J. Quevedo, M. McCormick, M. Wisher, R.D. Bengtson, T. Ditmire, Simultaneous streak and frame interferometry for electron density measurements of laser produced plasmas, *Rev. Sci. Instrum.* 87 (2016) 013107–5.
- [11] P. Nica, S. Gurlui, M. Osiac, M. Agop, M. Ziskind, C. Focsa, Investigation of femtosecond laser-produced plasma from various metallic targets using the Langmuir probe characteristic, *Phys. Plasmas* 24 (2017) 103119–10.
- [12] S.S. Harilal, C.V. Bindhu, R.C. Issac, V.P.N. Nampoori, C.P.G. Vallabhan, Electron density and temperature measurements in a laser produced carbon plasma, *J. Appl. Phys.* 82 (1997) 2140–2146.
- [13] H.R. Griem, Stark broadening of isolated spectral lines from heavy elements in a plasma, *Phys. Rev.* 128 (1962) 515–523.
- [14] H.R. Griem, *Plasma Spectroscopy*, McGraw-Hill, New York, 1964.
- [15] M. Hanif, M. Salik, F. Arif, Spectroscopic study of carbon plasma produced by the first (1064 nm) and second (532 nm) harmonics of Nd:YAG laser, *Plasma Phys. Rep.* 41 (2015) 274–280.
- [16] C. Sánchez Aké, H. Sobral, E. Sterling, M. Villagrán-Muniz, Time of flight of dual-laser ablation carbon plasmas by optical emission spectroscopy, *Appl. Phys. A* 79 (2004) 1345–1347.
- [17] F. Caridi, L. Torrisi, L. Giuffrida, Time-of-flight and UV spectroscopy characterization of laser-generated plasma, *Nucl. Instrum. Methods Phys. Res. B* 268 (2010) 499–505.
- [18] M.M. Abdelrahman, Factors enhancing production of multicharged ion sources and their applications, *Sci. Tech.* 2 (2012) 98–108.
- [19] E. Woryna, P. Parys, J. Wołowski, W. Mróz, Corpuscular diagnostics and processing methods applied in investigations of laser-produced plasma as a source of highly ionized ions, *Laser Part. Beams* 14 (1996) 293–321.
- [20] O. Balki, H.E. Elsayed-Ali, Multicharged carbon ion generation from laser plasma, *Rev. Sci. Instrum.* 87 (2016) 113304–10.
- [21] M.H.A. Shaim, M.M. Rahman, O. Balki, A. Sarkissian, M.L. Korwin-Pawłowski, H.E. Elsayed-Ali, Transport line for laser multicharged ion source, *Vacuum* 137 (2017) 14–22.
- [22] J.R. Freeman, S.S. Harilal, P.K. Diwakar, B. Verhoff, A. Hassanein, Comparison of optical emission from nanosecond and femtosecond laser produced plasma in atmosphere and vacuum conditions, *Spectrochim. Acta B* 87 (2013) 43–50.
- [23] G. Bekefi, *Principles of Laser Plasmas*, Wiley, New York, 1976.
- [24] S.S. Harilal, C.I. Riju, C.V. Bindhu, V.P.N. Nampoori, C.P.G. Vallabhan, Spatial analysis of C₂ band emission from laser produced plasma, *Plasma Sources. Sci. Technol.* 6 (1997) 317–322.
- [25] J.F. Ready, *Effects of High-Power Laser Radiation*, Academic Press, 1971.
- [26] F.J. Gordillo-Vázquez, A. Perea, A.P. McKiernan, C.N. Afonso, Electronic temperature and density of the plasma produced by nanosecond ultraviolet laser ablation of LiF, *Appl. Phys. Lett.* 86 (2005) 181501–3.
- [27] NIST Database. <http://physics.nist.gov/PhysRefData/ASD/index.html>.
- [28] P. Sankar, J.J.J. Nivas, N. Smijesh, G.K. Tiwari, R. Philip, Optical emission and dynamics of aluminum plasmas produced by ultrashort and short laser pulses, *J. Anal. Sci. Spectros.* 32 (2017) 1177–1185.
- [29] F.O. Bredice, D. Orzi, D. Schinca, H. Sobral, M. Villagrán-Muniz, Characterization of pulsed laser generated plasma through its perturbation in an electric field, *IEEE Trans. Plasma Sci.* 30 (2003) 2139–2143.
- [30] A. Ohzu, Y. Suzuki, Y. Maruyama, T. Arisawa, Enhancement of electron temperature in a laser-induced plasma using a radio-frequency electric field, *Phys. Plasmas* 7 (2000) 770–772.
- [31] D. Fried, T. Kushida, G.P. Reck, E.W. Rothe, The effects of the electric field associated with a laser-induced pulsed discharge on the ablation-generated plumes of YBa₂Cu₃O_{7-x}, *J. Appl. Phys.* 72 (1992) 1113–1125.
- [32] T. Mościcki, J. Hoffman, Z. Szymański, Modelling of plasma formation during nanosecond laser ablation, *Arch. Mech.* 63 (2011) 99–116.
- [33] N.M. Bulgakova, A.V. Bulgakov, O.F. Bobrenok, Double layer effects in laser-ablation plasma plumes, *Phys. Rev. E* 62 (2000) 5624–5635.
- [34] V.N. Rai, M. Shukla, H.C. Pant, Effect of chamber pressure induced space charge potential on ion acceleration in laser produced plasma, *Laser Part. Beams* 18 (2001) 315–324.
- [35] R. Kelly, R.W. Dreyfus, On the effect of Knudsen-layer formation on studies of vaporization, sputtering, and desorption, *Surf. Sci.* 198 (1988) 263–276.
- [36] H. Ryufuku, T. Watanabe, Total and partial cross sections for charge transfer in collisions of multicharged ions with atomic hydrogen, *Phys. Rev. A* 20 (1979) 1828–1837.
- [37] A. Lorusso, J. Krása, K. Rohlena, V. Nassisi, F. Belloni, D. Doria, Charge losses in expanding plasma created by an XeCl laser, *Appl. Phys. Lett.* 86 (2005) 081501–2.
- [38] J. Krása, K. Jungwirth, S. Gammino, E. Krouský, L. Láská, A. Lorusso, V. Nassisi, M. Pfeifer, K. Rohlena, L. Torrisi, J. Ullschmied, A. Velyhan, Partial currents of ion species in an expanding laser-created plasma, *Vacuum* 83 (2008) 180–184.
- [39] O. Balki, M.M. Rahman, S. Xiao, H.E. Elsayed-Ali, Generation of C⁶⁺ in a spark-discharge coupled laser plasma, *Opt. Commun.* 403 (2017) 50–54.
- [40] M.H.A. Shaim, F.G. Wilson, H.E. Elsayed-Ali, Aluminum multicharged ion generation from femtosecond laser plasma, *J. Appl. Phys.* 121 (2017) 185901–10.
- [41] Z. Qiushi, Y. Junzaburo, K. Nozomu, H. Tomonao, W. Masato, O. Akitoshi, H. Kazuhiko, H. Eiki, Structure and expansion characteristics of laser ablation tin plasma into a vacuum, Japan. *J. Appl. Phys.* 49 (2010) 056201–6.
- [42] A.M. Elsieid, N.C. Termini, P.K. Diwakar, A. Hassanein, Characteristics of ions emission from ultrashort laser produced plasma, *Sci. Rep.* 6 (2016) 38256.
- [43] V. Nassisi, L. Velardi, D. Delle Side, Electromagnetic and geometric characterization of accelerated ion beams by laser ablation, *Appl. Surf. Sci.* 272 (2013) 114–118.